Supporting Information

Self-Healing Liquid Metal Hydrogel for Human-Computer Interaction and Infrared Camouflage

Xiaofei Li,[ab] Miao Jiang,[ab] Yiming Du,[ab] Xin Ding,[a] Chao Xiao,[a] Yanyan Wang,[a] Yanyu Yang,[*c] Yizhi Zhuo,[a] Kang Zheng ,[a] Xianglan Liu,[a] Lin Chen,[a] Yi Gong,[a] Xingyou Tian,[ab] and Xian Zhang[*ab]

[a] *Key Lab of Photovoltaic and Energy Conservation Materials, Institute of Solid State Physics, HFIPS, Chinese Academy of Sciences, Hefei 230031, China*

[b] *University of Science and Technology of China, Hefei 230026, China*

[c]*College of Materials Science and Engineering, Zhengzhou University, Zhengzhou, Henan 450001, China*

**Corresponding authors at: 2221 Changjiang West Road, Shushan District, Hefei City, Anhui Province, People's Republic of China. E-mail addresses: xzhang@issp.ac.cn. 100 Science Avenue, Gaoxin District, Zhengzhou City, Henan Province, People's Republic of China. E-mail addresses: yyyang@zzu.edu.cn.*

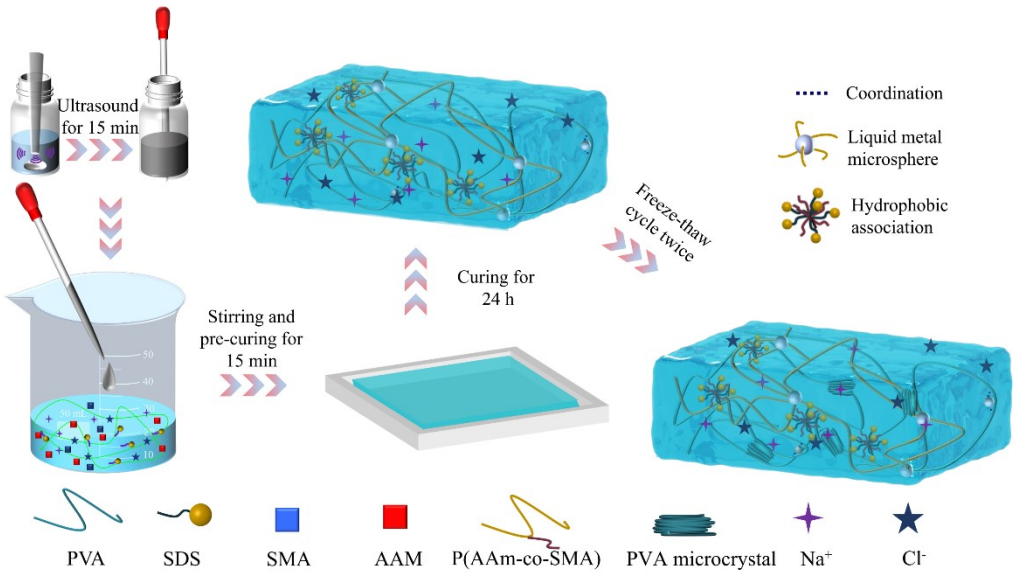

Fig. S1 Schematic diagram of the preparation process and structure of LM Hydrogel.

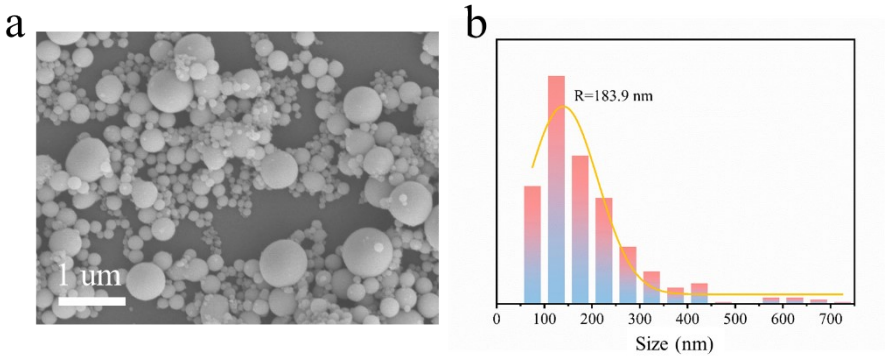

Fig. S2 (a) SEM image and (b) particle size distribution of LM (EGaIn) microspheres obtained by sonication for 15 minutes.

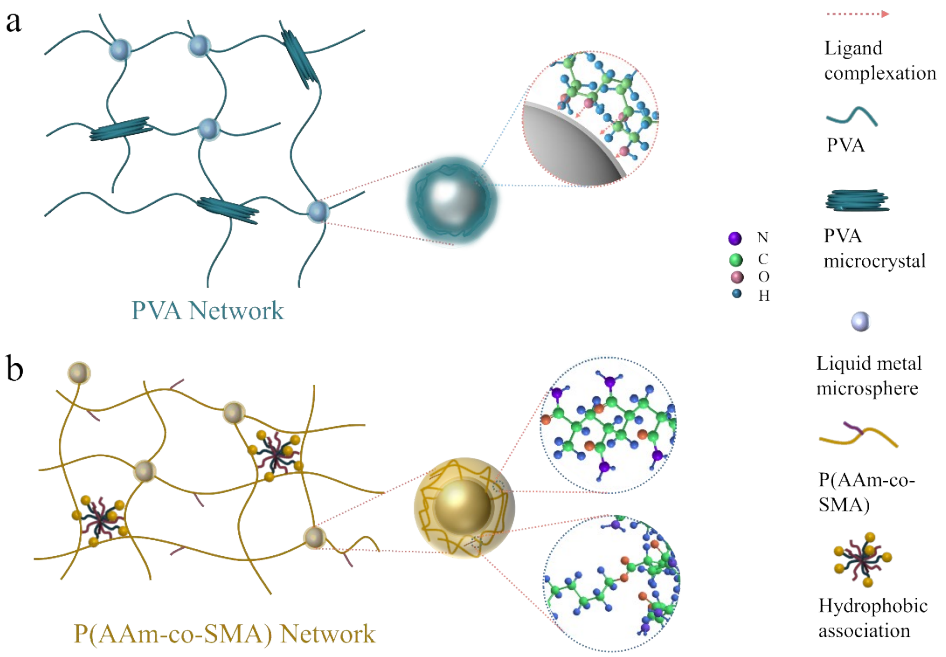

Fig. S3 Diagram of the crosslinked structures of (a) PVA network and (b) P(AAm-co-SMA) network.

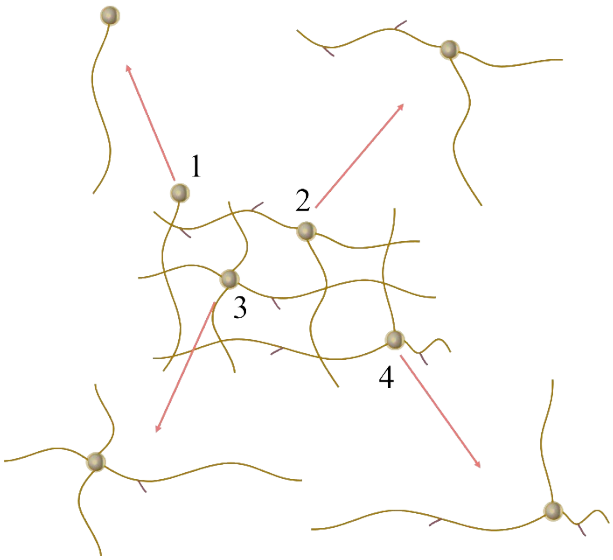

Fig. S4 The LM microspheres and the connected polymer chains occur slippage upon external mechanical deformation or pressure.

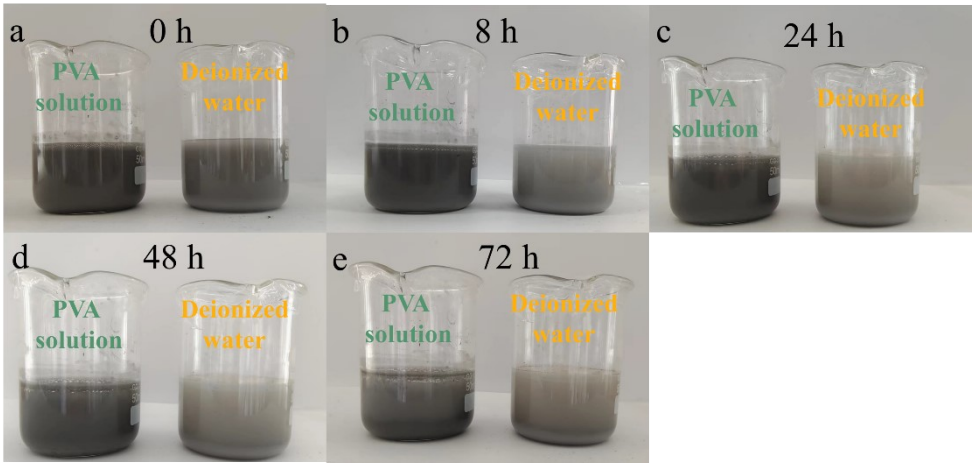

Fig. S5 Stability of LM microspheres in deionized water and aqueous PVA solutions after placing for (a) 0, (b) 8, (c) 24, (d) 48, (e) 72 h.

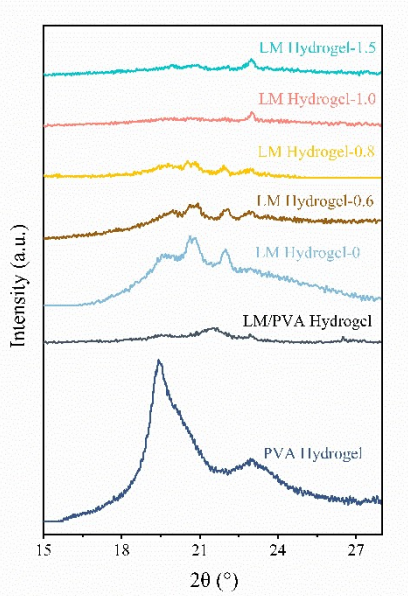

Fig. S6 XRD comparison plots of PVA, LM/PVA, and LM Hydrogels with different LM contents.

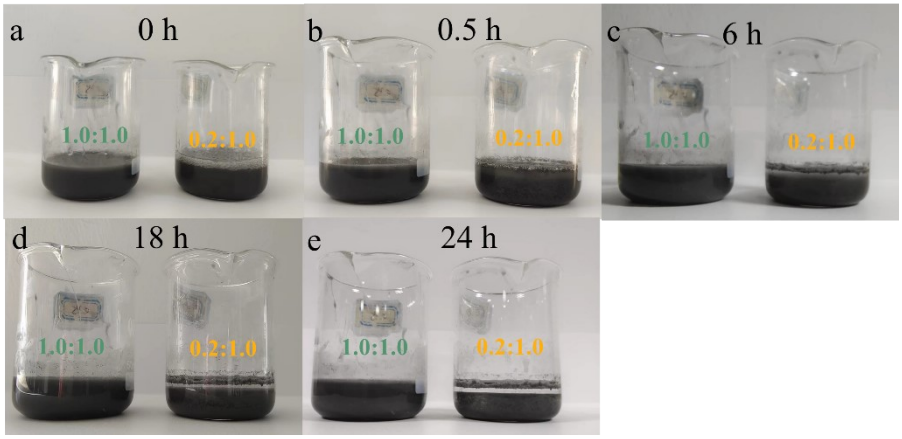

Fig. S7 The state of the hydrogel solution after (a) 0, (b) 0.5, (c) 6, (d) 18, and (e) 24 h when the ratio of LM to PVA is 0.2:1.0 and 1.0:1.0, respectively. When the ratio of LM to PVA is 0.2:1.0, the LM microspheres bind with PVA chains into a low-water-content hydrogel that precipitates from the aqueous solution, and the P(AAm-co-SMA) network was not successfully yielded. When the ratio of LM microspheres is 1.0:1.0, the polymerization rate is fast, and the P (AAm-co-SMA) network can be generated while forming a PVA network, resulting in a double-network LM Hydrogel.

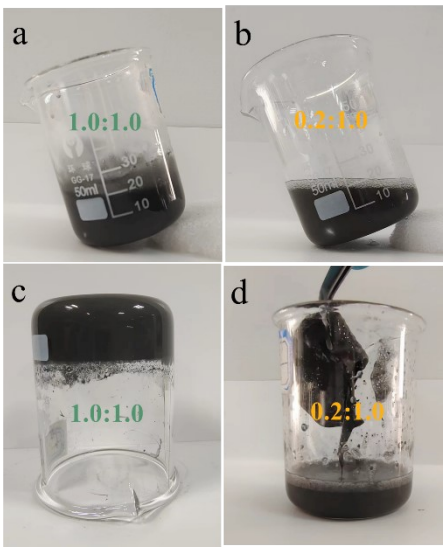

Fig. S8 (a, c) When the concentration of LM microspheres is 1.0:1.0, the P (AAm-co-SMA) network can be generated while forming a PVA network, resulting in a double-network LM Hydrogel. (b, d) When the ratio of LM to PVA is 0.2:1.0, the LM microspheres bind with PVA chains into a low-water-content hydrogel that precipitates from the aqueous solution.

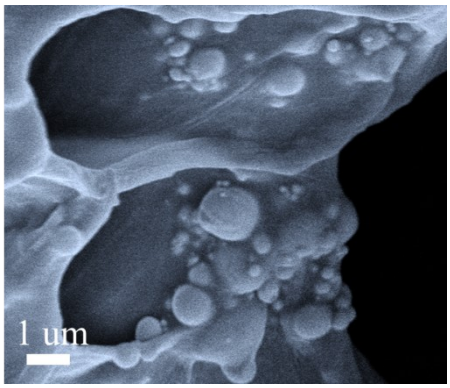

Fig. S9 The SEM image of the LM Hydrogel-1.0. The LM microspheres are encapsulated in the polymer matrix and the two phases of the hydrogel cannot be distinguished.

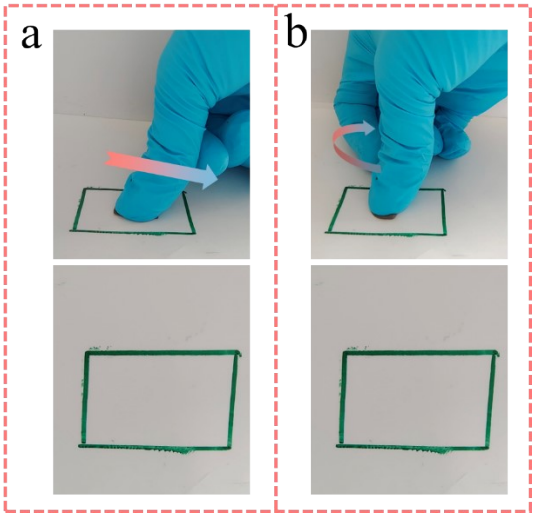

Fig. S10 The LM microspheres are encapsulated in the polymer matrix. The LM microspheres do not leak when the LM Hydrogel is (a) pressed or (b) rotated.

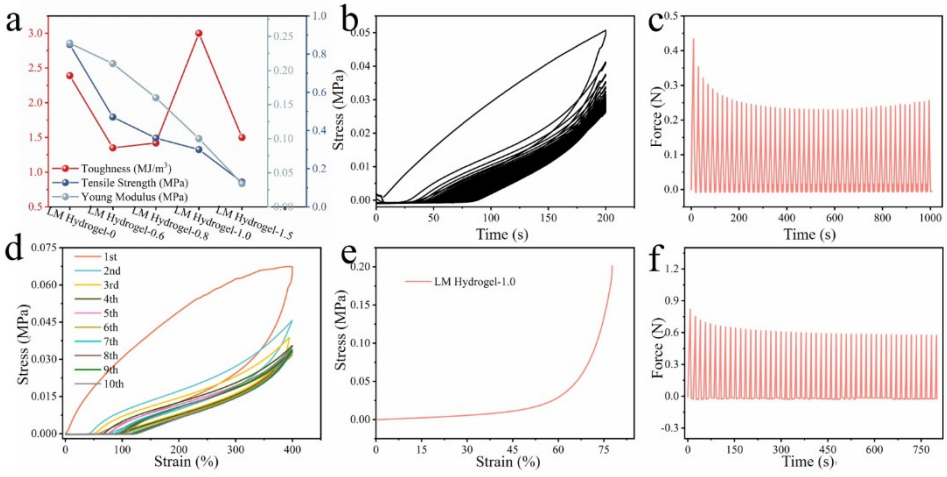

Fig. S11 (a) Young's modulus, tensile strength, and toughness of LM Hydrogel-n (n = 0, 0.6, 0.8, 1.0, and 1.5). (b) The stress-strain curve and (c) force-time curve of LM Hydrogel-1.0 during consecutive 50 elongation-relaxation cycles at the strain of 200%. (d) The stress-strain curve of LM Hydrogel-1.0 during consecutive 10 elongation-relaxation cycles at the strain of 400%. (e) Compressive stress-strain curve of LM Hydrogel-1.0. (f) The force-time curve of LM Hydrogel-1.0 during consecutive 50 compression-relaxation cycles at the strain of 30%.

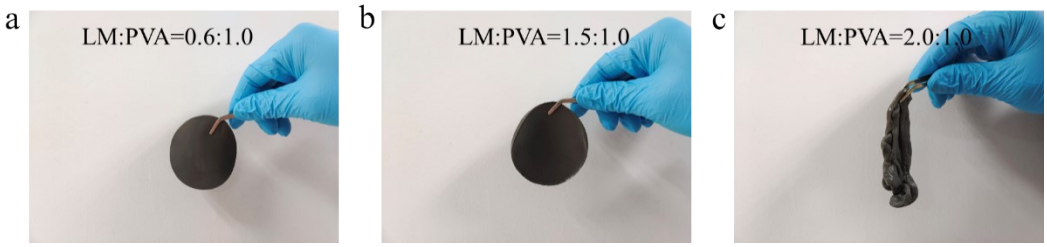

Fig. S12 LM Hydrogels with various ratios of LM to PVA: (a) 0.6:1.0, (b) 1.5:1.0, and (c) 2.0:1.0.

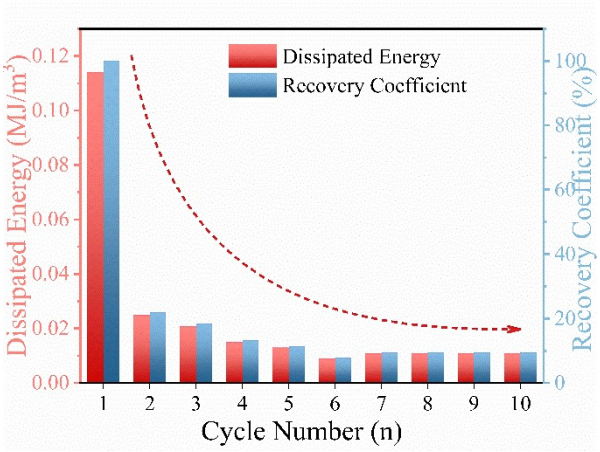

Fig. S13 Dissipation energy and recovery efficiency of the hydrogel during 10 cycles at a strain of 400%.

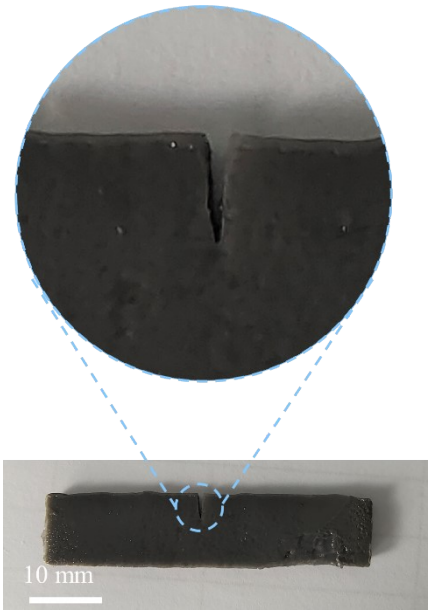

Fig. S14 LM Hydrogel strip cut out a notch with a width of 1/3 of the strip width.

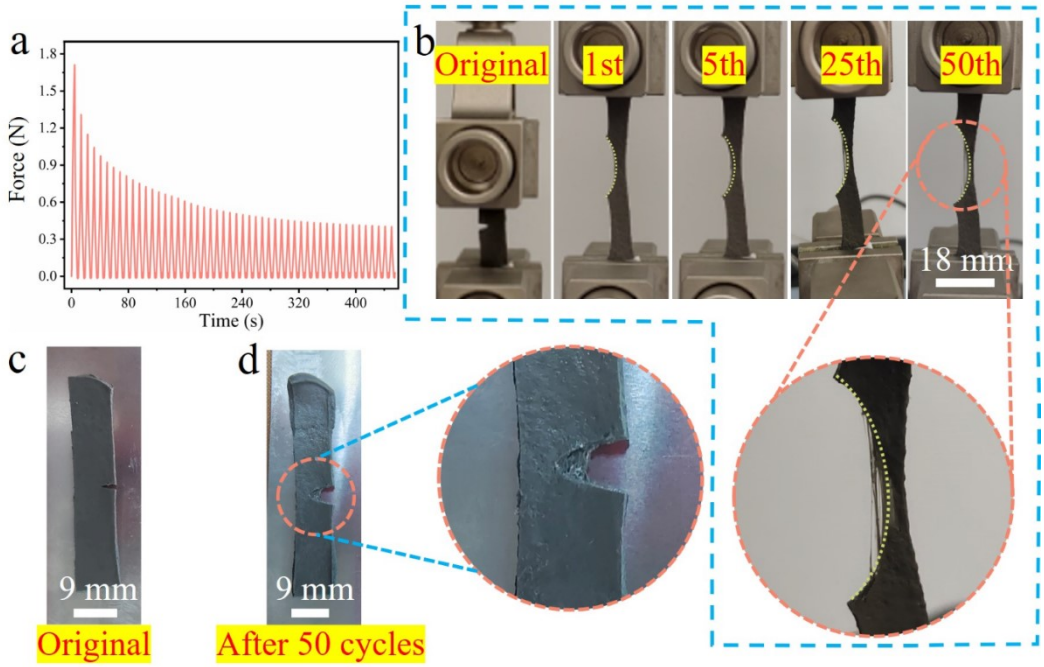

Fig. S15 (a) Force-time curve of notched LM Hydrogel during consecutive 50 elongation-relaxation cycles. (b) Photographs of notched LM Hydrogel during the elongation-relaxation cycles. (c,d) Photographs of notched LM Hydrogel before and after the 50 cycles.

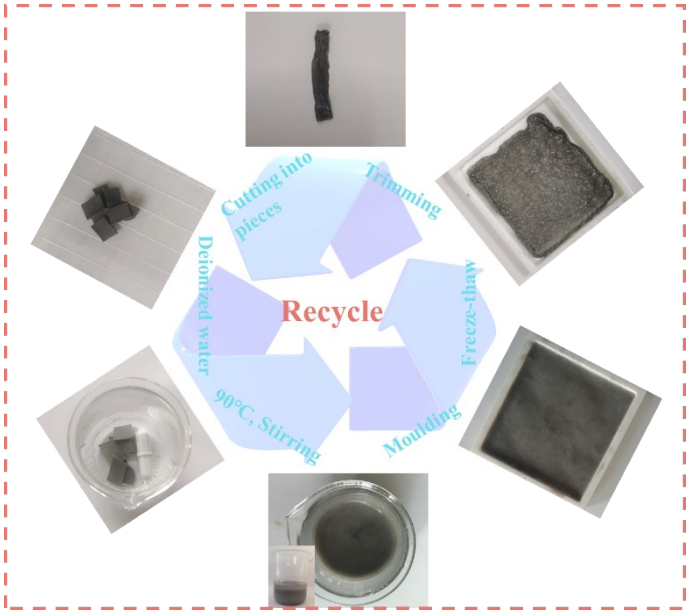

Fig. S16 Recyclability of LM Hydrogel with multiple physical cross-links.

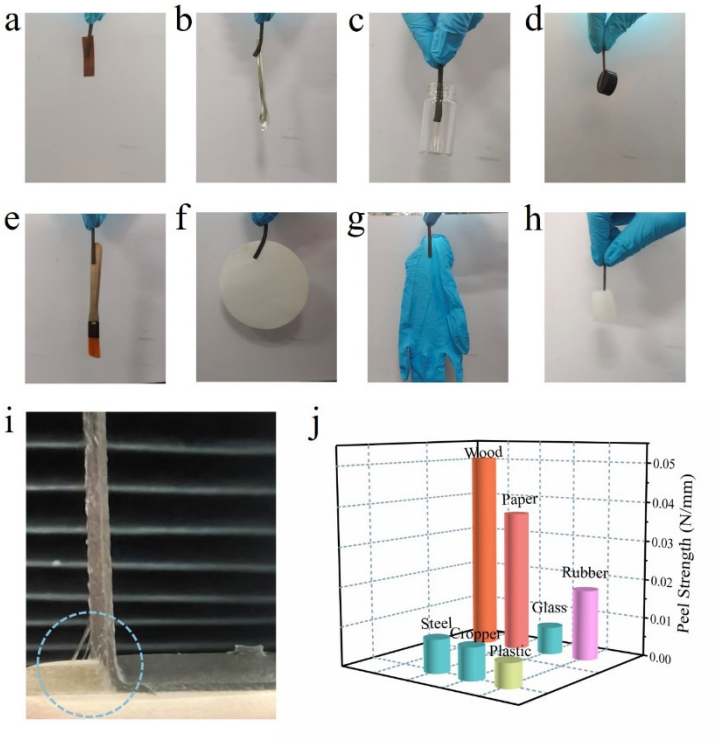

Fig. S17 LM Hydrogel can adhere to (a) copper, (b) stainless steel, (c) glass, (d) plastic, (e) wood, (f) paper, and (g, h) rubber. (i) Photograph of 90 ° peel test of LM Hydrogel from the wood plate. (j) Peel strengths of LM Hydrogel on various materials.

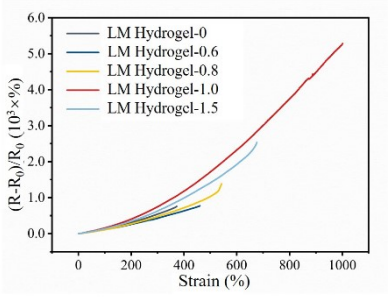

Fig. S18 Real-time relative resistance variation of the LM Hydrogels with different LM contents during the stretching process.

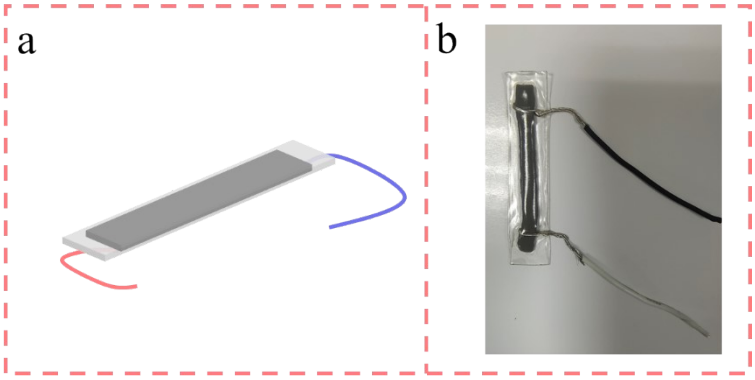

Fig. S19 (a) Schematic diagram and (b) photo of the strain sensor prepared by encapsulating the LM Hydrogel and electrode with 3M tape.

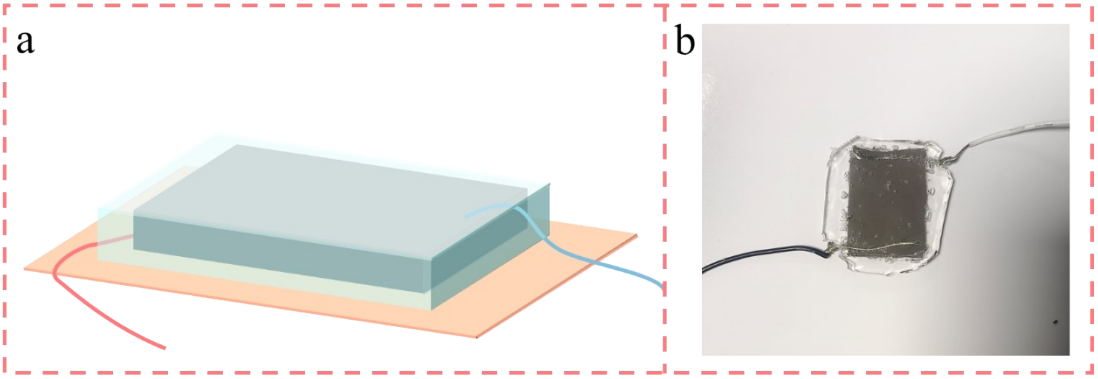

Fig. S20 (a) Schematic diagram and (b) photo of the pressure sensor prepared by encapsulating the LM Hydrogel and electrode with PDMS.

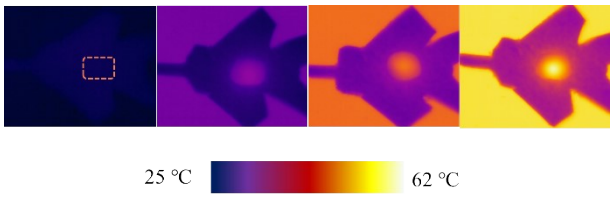

Fig. S21 The infrared camouflage effect of the fighter model covered by the photothermal LM Hydrogel with various temperatures.

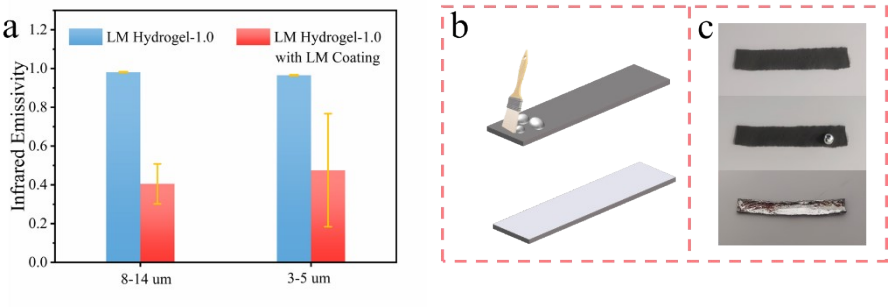

Fig. S22 (a) The infrared emissivity of LM Hygrogel-1.0 and LM Hygrogel-1.0 with LM coating in the atmospheric window (3-5 um, 8-14 um). (b, c) The LM can be uniformly coated on the LM Hydrogel.

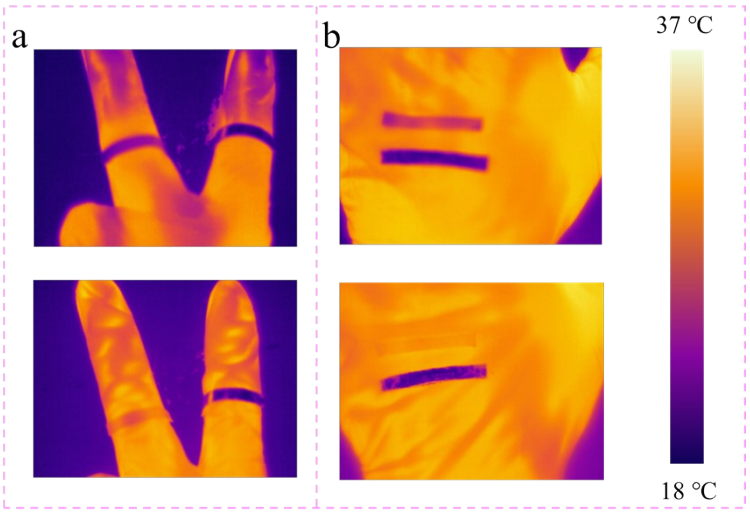

Fig. S23 (a) The infrared images of the LM Hydrogel and LM Hydrogel with LM coating worn on fingers. (b) The infrared images of the LM Hydrogel and LM Hydrogel with LM coating attached to the back of the hand.